Oxygen-Reduction Reaction Hot Paper

International Edition: DOI: 10.1002/anie.201509024
German Edition: DOI: 10.1002/ange.201509024

# A Versatile Iron–Tannin-Framework Ink Coating Strategy to Fabricate Biomass-Derived Iron Carbide/Fe-N-Carbon Catalysts for Efficient Oxygen Reduction

*Jing Wei, Yan Liang, Yaoxin Hu, Biao Kong, George P. Simon, Jin Zhang, San Ping Jiang, and Huanting Wang**

***Abstract:*** *The conversion of biomass into valuable carbon composites as efficient non-precious metal oxygen-reduction electrocatalysts is attractive for the development of commercially viable polymer electrolyte membrane fuel-cell technology. Herein, a versatile iron–tannin-framework ink coating strategy is developed to fabricate cellulose-derived $Fe_3C$/Fe-N-C catalysts using commercial filter paper, tissue, or cotton as a carbon source, an iron–tannin framework as an iron source, and dicyandiamide as a nitrogen source. The oxygen reduction performance of the resultant $Fe_3C$/Fe-N-C catalysts shows a high onset potential (i.e. 0.98 V vs the reversible hydrogen electrode (RHE)), and large kinetic current density normalized to both geometric electrode area and mass of catalysts (6.4 mA $cm^{-2}$ and 32 mA $mg^{-1}$ at 0.80 V vs RHE) in alkaline condition. This method can even be used to prepare efficient catalysts using waste carbon sources, such as used polyurethane foam.*

The polymer-electrolyte membrane fuel cell is one of promising clean power sources to convert chemical energy directly into electrical energy.[1] Catalysts for its cathode reaction (i.e. oxygen-reduction reaction; ORR) are one of the key components in fuel cell, and are usually Pt-based materials which are required to overcome the sluggish kinetics of ORR.[2] However, such Pt-based catalysts suffer some drawbacks, such as their high cost, limited resource, low CO and methanol tolerance, and poor durability, which limit the commercialization of fuel cells. Recently, composite carbon materials with N and earth-abundant transition-metal doping (i.e. Fe-N-C)[3] or encapsulated nanoparticles by a graphitic carbon layer (i.e. $Fe/Fe_3C$/C)[4] have been considered as the most promising non-precious metal catalysts for ORR owing to their superior catalytic activity and stability, easy availability, and low cost. Their active sites are believed to be iron coordinated with nitrogen doping in carbon (Fe-N-C), as well as graphitic carbon layers activated by the encapsulated iron and (or) iron carbide nanoparticles ($Fe/Fe_3C$/C). The most widely used method for the preparation of such catalysts involves direct pyrolysis of the composites of carbon, nitrogen, and metal precursors. Tremendous efforts have been focused on the choice of different carbon, nitrogen, and metal sources, and tailoring the nanostructures to achieve a catalytic performance comparable to commercial Pt/C catalysts. However, most of these catalysts are based on nanostructured carbon (such as, graphene or carbon nanotubes), and are prepared via complicated procedures.[5] The development of a sustainable route to prepare efficient catalysts using renewable precursors is highly desirable for the widespread commercialization of fuel cells.

Recently, the conversion of biomass into valuable porous carbon materials for energy storage and conversion has attracted increasing attention owing to the ever-increasing demand for the conversion and storage of renewable energy.[6] A variety of biomass have been explored as the source of carbon catalysts for ORR.[7] Generally, the carbon composites derived from biomass show low catalytic performance owing to the low degree of graphitization, high yield of by-products (such as unsealed metal nanoparticles on carbon surface), low nitrogen content, and low density of catalytic sites (i.e. M-N-C). To address these problems, different strategies have been developed to increase the catalytic performance of biomass-derived carbon, such as the incorporation of iron species into the biomass during carbonization to increase the degree of graphitization, and activation under ammonia to increase the porosity and N content in the carbon skeleton.[8] However, there is still an urgent need to develop a universal method to prepare biomass-derived carbon with high catalytic performance.

Herein, we report on a versatile iron–tannin-framework "ink" coating strategy to fabricate high-performance $Fe_3C$/Fe-N-C catalysts for ORR by coating an organic iron source onto cellulose fibers, followed by grinding with dicyandiamide, carbonization, and acid etching. Cellulose is chosen as the carbon source because it is the most abundant biomass. Dicyandiamide (DCDA), a low-cost material, is used as the N source owing to its high nitrogen content (61 wt%). The concept for the fabrication of carbon catalysts is to develop an iron–tannin-framework ink as the organic iron source. Compared with the inorganic iron source (i.e. $Fe(NO_3)_3$), the iron–tannin-framework ink can be uniformly coated on

[*] Dr. J. Wei, Y. Liang, Y. Hu, B. Kong, Prof. H. Wang
Department of Chemical Engineering
Monash University
Clayton, Victoria 3800 (Australia)
E-mail: huanting.wang@monash.edu
Prof. G. P. Simon
Department of Materials Engineering, Monash University
Clayton, Victoria 3800 (Australia)
J. Zhang, Prof. S. P. Jiang
Fuels and Energy Technology Institute & Department of Chemical Engineering, Curtin University
Perth, WA 6102 (Australia)

Supporting information for this article is available on the WWW under http://dx.doi.org/10.1002/anie.201509024.

  

various organic substrates, such as biomass, promoting the formation of active sites (Fe-N-C and $Fe_3C$/C). Different cellulose fiber-based products, such as filter paper, tissue, and cotton as well as other low-cost products, such as polyurethane-foam waste were used as the carbon source. Their derived carbons show high catalytic activities for ORR. To our knowledge, this is the first time a metal–organic-framework ink coating method has been used for the preparation of high-performance oxygen reduction catalysts using commercial and low-cost products as carbon sources.

Tannic acid (TA) is a low-cost and environmentally friendly polyphenol, and widely distributed in plant tissues. Its chemical structure is shown in Figure 1a. TA is also a versatile coating molecule as it can strongly bind to substrates with different shapes (such as, film and particle)

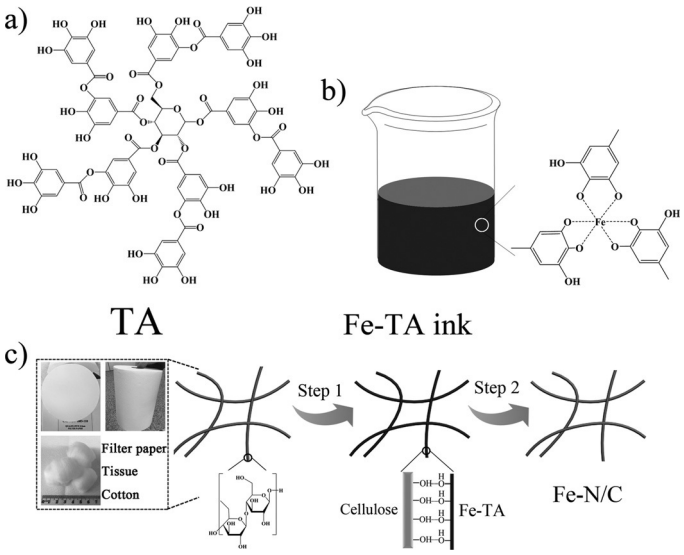


***Figure 1.*** a) Chemical structure of tannic acid (TA); b) Schematic representation of Fe-TA-framework ink in a beaker and chemical structure of the ink; c) The procedures for the preparation of catalyst: Step 1, coating the Fe-TA-framework ink onto the surface of cellulose fibers from commercial products, such as filter paper, tissue paper, and cotton; Step 2, the carbonization of cellulose/Fe-TA composites combined with dicyandiamide as a nitrogen source, followed by acid leaching to remove the exposed iron-base nanoparticles.

and surface properties (hydrophilic or hydrophobic) through covalent and noncovalent interactions.[9] Additionally, TA can coordinate with various metal ions to form a stable metal–tannin framework via a strong interaction between metal ions and catechols. The iron–tannin-framework ink (Figure 1b) was prepared by simply mixing tannic acid and Fe-$(NO_3)_3{\cdot}9H_2O$ in water (denoted Fe-TA). This Fe-TA ink looks similar to the commercial iron gall ink, which was widely used for writing and drawing. Because of its excellent penetrability and adhesion (Figure S1 in the Supporting Information), Fe-TA ink could be employed as a coating material by using printing or spraying techniques.

The preparation of catalysts involves two steps (Figure 1c). Firstly, Fe-TA ink was coated on the surface of the cellulose fibers. Secondly, the cellulose/Fe-TA composites were mixed with DCDA by grinding, carbonized, and leached by 2 M HCl to give the composite carbon catalysts. During the carbonization, DCDA and its derived species (i.e. melamine) would react with TA molecules to form N-doped carbon.[10]

Filter paper (denoted FP) was chosen as a typical cellulose source owing to its porous structure (Figure S2). Transmission electron microscopy (TEM) image of filter-paper-derived composite carbon (denoted FP-Fe-TA-N-850) revealed that the $Fe_3C$ nanoparticles were embedded in the carbon matrix (Figure 2a). As $Fe_3C$ nanoparticles are unstable in acid, they should be removed after acid leaching. However, many $Fe_3C$ nanoparticles were retained after acid leaching. A high-resolution TEM image confirmed that $Fe_3C$ nanoparticles were encapsulated by the graphitic carbon layer, which protects the $Fe_3C$ nanoparticles from acid etching (Figure 2b). Previous research demonstrated that the encapsulated $Fe_3C$ nanoparticles could activate the graphitic carbon layer and make the surrounding carbon active for ORR.[4d] This kind of graphitic layer would enhance the catalytic performance when combined with Fe-N-C species. A scanning transmission electron microscopy (STEM) image further confirmed that $Fe_3C$ nanoparticles were dispersed in the carbon matrix uniformly (Figure 2c). The energy-dispersive X-ray spectroscopy clearly showed the existence of N, O, and Fe elements in the carbon matrix (Figure S3). The element mapping results revealed that both nitrogen and oxygen were distributed in the carbon matrix uniformly, indicating the nitrogen atoms were successfully doped into the carbon lattice. The strong Fe element signals mainly existed in the area of nanoparticles (white dots in Figure 2c), confirming the formation of $Fe_3C$ during carbonization (Figure 2d–g). To demonstrate the versatility of such a coating method, other cellulose-based commercial products, such as tissue and cotton were also used as the carbon source. Their SEM and TEM images showed similar results (Figure S4,S5).

X-ray diffraction (XRD) patterns showed the phase of cellulose was changed to $Fe_3C$ and graphite after carbonization (Figure S6). All other carbon composites, such as FP-Fe-N-850 (iron nitrate as the Fe source), TS-Fe-TA-N-850 and c-Fe-TA-N-850 (tissue (TS) and cotton (c) as the carbon source) also showed $Fe_3C$ and graphite phase. $N_2$ sorption analysis was used to determine the specific surface area and pore size of the obtained carbon (Figure S7). Their specific surface areas were 16, 104, 106, and 202 $m^2 g^{-1}$ for FP-Fe-TA-N-850, FP-Fe-N-850, TS-Fe-TA-N-850 and c-Fe-TA-N-850, respectively.

X-ray photoelectron spectroscopy (XPS) for FP-Fe-TA-N-850 further showed the existence of Fe and N, with a content of 0.14 and 7.23 at%, respectively (Figure S8a,b). The iron content was low because the iron carbide nanoparticles were covered by graphitic carbon and thus could not be detected. Note that pyridinic nitrogen and pyrrolic nitrogen atoms can coordinate with Fe to form Fe-$N_x$ active site. The N 1s spectra for FP-Fe-TA-N-850 were fitted with four peaks at about 398.4, 399.3, 400.9, and 403.6 eV, corresponding to pyridinic nitrogen, pyrrolic nitrogen, graphitic nitrogen, and pyridinic $N^+$–$O^-$, respectively (Figure S8c). Their rela-

  

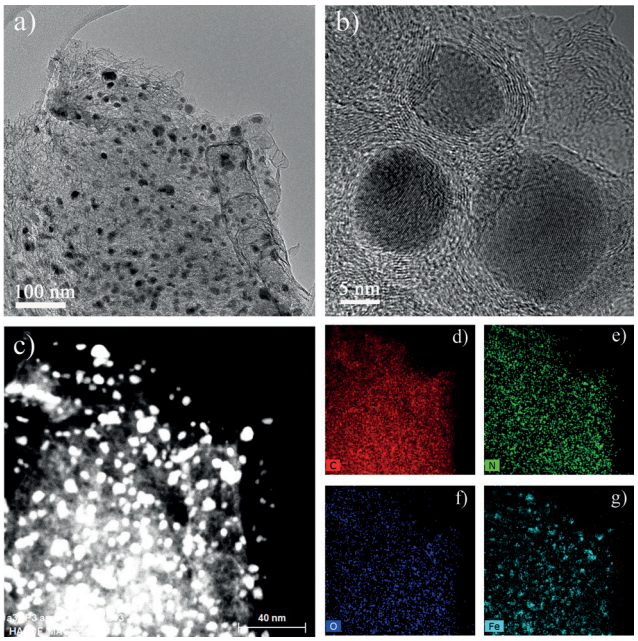


***Figure 2.*** a,b) TEM images of FP-Fe-TA-N-850. c) STEM image of FP-Fe-TA-N-850, and d)–g) its corresponding elements mapping images: d) C, e) N, f) O, g) Fe.

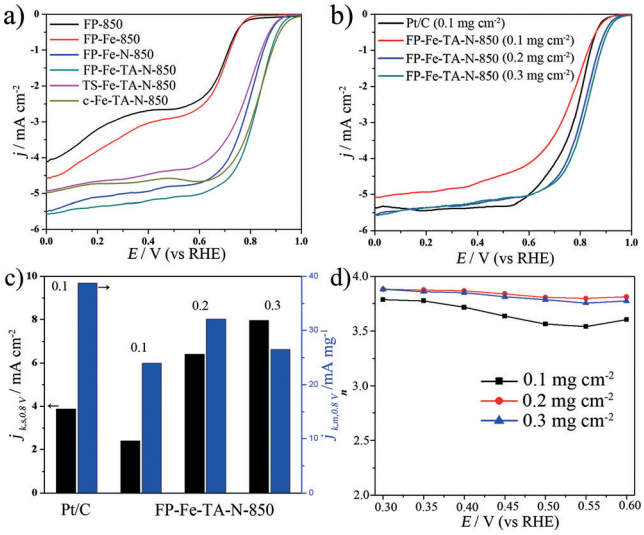


***Figure 3.*** a) LSV curves of FP-850, FP-Fe-850, FP-Fe-N-850, FP-Fe-TA-N-850, TS-Fe-TA-N-850, and c-Fe-TA-N-850 at 1600 rpm in $O_2$ saturated 0.1 M KOH solution (the loading is 0.3 mg cm$^{-2}$); b) LSV curves of Pt/C and FP-Fe-TA-N-850 with different loadings (0.1, 0.2, 0.3 mg cm$^{-2}$); c) The kinetic current density normalized to both electrode surface area (black) and mass of the catalysts (blue) measured at 0.80 V (vs RHE); The unit of loading is mg cm$^{-2}$; and d) The electron transfer numbers of FP-Fe-TA-N-850 with different loadings.

tive contents were 28.13, 21.10, 32.61, and 18.17%, respectively (Figure S8c,d).

The ORR performance of the catalysts was evaluated using a rotating disk electrode (RDE) technique. Cyclic voltammetry (CV) and linear scan voltammogram (LSV) curves of FP-Fe-TA-N-*x* carbonized at different temperatures ($x = 800$, 850, 900, and 950 °C) showed that the catalytic performance of FP-Fe-TA-N-850 is the best among these samples. Therefore, 850 °C was chosen to carbonize other cellulose/Fe/N composites for further investigations (Figure S9). To demonstrate the roles of Fe and N source in the ORR, FP-850, FP-Fe-850, and FP-Fe-N-850 were prepared by direct carbonization of filter paper, filter paper/iron nitrate and filter paper/iron nitrate/DCDA with the same procedure as FP-Fe-TA-N-850. LSV curves of both FP-850 and FP-Fe-850 showed a low onset potential ($E_{onset}$) and limiting current density ($j_L$; Figure 3a). However, after incorporating both iron and nitrogen sources, an obvious increase in both $E_{onset}$ and $j_L$ was observed for FP-Fe-N-850, indicating the iron and nitrogen species have a synergetic effect in enhancing catalytic performance. Notably, FP-Fe-TA-N-850 revealed an even more positive $E_{onset}$ (0.98 V vs RHE) and larger $j_L$ (5.0 mA cm$^{-2}$ at 0.60 V) than FP-Fe-N-850. As both FP-Fe-N-850 and FP-Fe-TA-N-850 were prepared using the same carbon source (filter paper), nitrogen source (DCDA), and carbonization procedure, and FP-Fe-TA-N-850 had a lower specific surface area than FP-Fe-N-850, the enhanced catalytic performance for FP-Fe-TA-N-850 was mainly a result of the use of organic iron sources. The use of the organic iron source (Fe-TA) may be beneficial for forming graphitic layers activated by encapsulated $Fe_3C$ nanoparticles.

The catalysts derived from tissue paper and cotton also showed a high catalytic performance (Figure 3a, S10, S11), indicating that Fe-TA ink coating is a versatile method to fabricate efficient catalysts using different cellulose fibers as carbon sources. This coating method could also be used to fabricate catalysts using other low-cost and easily available supports. For example, the polyurethane-foam (sponge) waste derived catalysts still showed a high catalytic performance (Figure S12).

FP-Fe-TA-N-850 also revealed comparable catalytic performance to Pt/C at the same loading (i.e. 0.1 mg cm$^{-2}$), and higher performance than commercial Pt/C (20 wt%, Sigma–Aldrich) when their loadings were two- and three-times that of Pt/C in alkaline conditions (Figure S13, Figure 3b). Note that the catalysts were prepared using commercial cellulose-based material (filter paper) as the carbon source. However, the ORR performance is still among the best of non-precious metal catalyst reported to date, even comparable with some non-precious metal catalysts using nanocarbon as carbon source (Table S1).

Although the catalyst precursors were much cheaper than Pt/C (Figure S14), and increasing the loading of the catalysts could be an alternative way to achieve high performance comparable to Pt/C, the potential issue for mass transfer may arise. The kinetic current densities normalized to both geometrical electrode surface area ($j_{k,s}$) and mass ($j_{k,m}$) of the catalysts at 0.80 V (vs RHE) were further determined (Figure 3c). When the loading was 0.1, 0.2, and 0.3 mg cm$^{-2}$, $j_{k,s}$ increased from 2.4 to 8.0 mA cm$^{-2}$. The highest $j_{k,m}$ was 32 mA mg$^{-1}$ when the loading is 0.2 mg cm$^{-2}$, which was close to that of Pt/C (38.7 mA mg$^{-1}$). The average turnover frequency (TOF) of FP-Fe-TA-N-850 on the basis of the Fe-$N_x$/C active sites is estimated to be around 3.0 e site$^{-1}$ s$^{-1}$, indicating that this catalyst has high catalytic activity (Fig-

  

ure S15). The electron-transfer number per oxygen molecule ($n$) calculated from Koutechy–Levich equation was around 3.5–3.9, indicating a dominate 4e pathway for ORR (Figure 3d, Figure S16). A higher loading favored a 4e process and decreased the yield of by-products (i.e. $H_2O_2$). FP-Fe-TA-N-850 also showed a better long-term stability and higher resistance to the methanol crossover effect than Pt/C (Figure S17). In addition, FP-Fe-TA-N-850 showed good ORR performance in acid conditions (Figure S18, Table S2).

As cellulose contains no nitrogen and their derived carbon shows a low degree of graphitization (Figure S19), the successful incorporation of N and Fe sources uniformly on the cellulose fiber is the key to the preparation of high-performance catalysts. Based on the above results, we attribute the high ORR performance to the efficient carbon, nitrogen, and iron sources chosen. The carbon sources allow for the uniform loading of nitrogen and iron sources, which is a possible because of their highly porous structure. DCDA is highly reactive with these carbon sources during carbonization. Most importantly, the Fe-TA-framework ink is shown to be an excellent iron precursor for high-performance catalysts. When inorganic iron sources are used, the iron ions adsorbed on the surface of cellulose tend to aggregate easily during the carbonization and fail to form a high density of active sites. In contrast, the Fe-TA framework can be firmly coated on the cellulose fibers through the good adhesion of TA. As the iron ions were trapped in the framework of TA, encapsulated $Fe_3C$ nanoparticles could be easily formed. In addition, nitrogen was easier to dope in the organic iron source. The active sites of $Fe_3C$-C and Fe-N-C may act with a synergetic catalytic effect in enhancing the catalytic performance.[3i]

In conclusion, a versatile iron–tannin-framework ink-coating strategy has been demonstrated for the fabrication of high-performance $Fe_3C$/Fe-N-C catalysts for the oxygen reduction reaction by using the low-cost, easily available cellulose fiber-based commercial materials (filter paper, tissue, and cotton), even polyurethane-foam waste as the carbon sources. This ink is suitable for large-scale fabrication of high-performance electrocatalysts using different industry-standard processes, such as printing or spray coating. As a result of the strong interactions between metal ions and TA, it should be possible to prepare other metal–tannin-framework inks, such as Co-TA, Ni-TA, and Cu-TA for synthesizing other metal (or metal oxide, metal carbide)/carbon composites for supercapacitors, batteries, and catalysts.

## Acknowledgements

This work is supported by the Australian Research Council through Discovery grants (Project No. DP150100765 and DP150102044). We acknowledge the use of equipment, scientific and technical assistance of the WA X-Ray Surface Analysis Facility, funded by the Australian Research Council LIEF grant LE120100026.

**Keywords:** biomass · carbon · metal–tannin framework · non-precious metal catalysts · oxygen reduction reaction

**How to cite:** *Angew. Chem. Int. Ed.* **2016**, *55*, 1355–1359
*Angew. Chem.* **2016**, *128*, 1377–1381

[1] a) B. C. H. Steele, A. Heinzel, *Nature* **2001**, *414*, 345–352; b) R. Bashyam, P. Zelenay, *Nature* **2006**, *443*, 63–66; c) M. K. Debe, *Nature* **2012**, *486*, 43–51.

[2] a) Z. Chen, D. Higgins, A. Yu, L. Zhang, J. Zhang, *Energy Environ. Sci.* **2011**, *4*, 3167–3192; b) H. A. Gasteiger, S. S. Kocha, B. Sompalli, F. T. Wagner, *Appl. Catal. B* **2005**, *56*, 9–35; c) F. Jaouen, E. Proietti, M. Lefevre, R. Chenitz, J.-P. Dodelet, G. Wu, H. T. Chung, C. M. Johnston, P. Zelenay, *Energy Environ. Sci.* **2011**, *4*, 114–130; d) D.-W. Wang, D. Su, *Energy Environ. Sci.* **2014**, *7*, 576–591; e) Y. Nie, L. Li, Z. D. Wei, *Chem. Soc. Rev.* **2015**, *44*, 2168–2201; f) L. Dai, Y. Xue, L. Qu, H.-J. Choi, J.-B. Baek, *Chem. Rev.* **2015**, *115*, 4823–4892.

[3] a) C. W. B. Bezerra, L. Zhang, K. Lee, H. Liu, A. L. B. Marques, E. P. Marques, H. Wang, J. Zhang, *Electrochim. Acta* **2008**, *53*, 4937–4951; b) M. Lefèvre, E. Proietti, F. Jaouen, J. Dodelet, *Science* **2009**, *324*, 71–74; c) G. Wu, K. L. More, C. M. Johnston, P. Zelenay, *Science* **2011**, *332*, 443–447; d) S. Guo, S. Zhang, S. Sun, *Angew. Chem. Int. Ed.* **2013**, *52*, 8526–8544; *Angew. Chem.* **2013**, *125*, 8686–8705; e) J. Liang, R. F. Zhou, X. M. Chen, Y. H. Tang, S. Z. Qiao, *Adv. Mater.* **2014**, *26*, 6074–6079; f) Y. Zhu, B. Zhang, X. Liu, D.-W. Wang, D. S. Su, *Angew. Chem. Int. Ed.* **2014**, *53*, 10673–10677; *Angew. Chem.* **2014**, *126*, 10849–10853; g) Z. Li, G. Li, L. Jiang, J. Li, G. Sun, C. Xia, F. Li, *Angew. Chem. Int. Ed.* **2015**, *54*, 1494–1498; *Angew. Chem.* **2015**, *127*, 1514–1518; h) W. Niu, L. Li, X. Liu, N. Wang, J. Liu, W. Zhou, Z. Tang, S. Chen, *J. Am. Chem. Soc.* **2015**, *137*, 5555–5562; i) Z.-Y. Wu, X.-X. Xu, B.-C. Hu, H.-W. Liang, Y. Lin, L.-F. Chen, S.-H. Yu, *Angew. Chem. Int. Ed.* **2015**, *54*, 8179–8183; *Angew. Chem.* **2015**, *127*, 8297–8301; j) M. Xiao, J. Zhu, L. Feng, C. Liu, W. Xing, *Adv. Mater.* **2015**, *27*, 2521–2527; k) W. Yang, X. Liu, X. Yue, J. Jia, S. Guo, *J. Am. Chem. Soc.* **2015**, *137*, 1436–1439; l) J. Wei, Y. Hu, Z. Wu, Y. Liang, S. Leong, B. Kong, X. Zhang, D. Zhao, G. P. Simon, H. Wang, *J. Mater. Chem. A* **2015**, *3*, 16867–16873; m) J. Wei, Y. Liang, X. Zhang, G. P. Simon, D. Zhao, J. Zhang, S. Jiang, H. Wang, *Nanoscale* **2015**, *7*, 6247–6254; n) J. Wei, Y. Hu, Y. Liang, B. Kong, J. Zhang, J. Song, Q. Bao, G. P. Simon, S. P. Jiang, H. Wang, *Adv. Funct. Mater.* **2015**, *25*, 5768–5777.

[4] a) Z. Wen, S. Ci, F. Zhang, X. Feng, S. Cui, S. Mao, S. Luo, Z. He, J. Chen, *Adv. Mater.* **2012**, *24*, 1399–1404; b) J.-S. Lee, G. S. Park, S. T. Kim, M. Liu, J. Cho, *Angew. Chem. Int. Ed.* **2013**, *52*, 1026–1030; *Angew. Chem.* **2013**, *125*, 1060–1064; c) D. Deng, L. Yu, X. Chen, G. Wang, L. Jin, X. Pan, J. Deng, G. Sun, X. Bao, *Angew. Chem. Int. Ed.* **2013**, *52*, 371–375; *Angew. Chem.* **2013**, *125*, 389–393; d) Y. Hu, J. O. Jensen, W. Zhang, L. N. Cleemann, X. Wei, N. J. Bjerrum, Q. Li, *Angew. Chem. Int. Ed.* **2014**, *53*, 3675–3679; *Angew. Chem.* **2014**, *126*, 3749–3753; e) J. Masa, W. Xia, M. Muhler, W. Schuhmann, *Angew. Chem. Int. Ed.* **2015**, *54*, 10102–10120; *Angew. Chem.* **2015**, *127*, 10240–10259.

[5] a) Q. Li, R. Cao, J. Cho, G. Wu, *Adv. Energy Mater.* **2014**, *4*, 1301415; b) X. Zhou, J. Qiao, L. Yang, J. Zhang, *Adv. Energy Mater.* **2014**, *4*, 1301523; c) G. Wu, P. Zelenay, *Acc. Chem. Res.* **2013**, *46*, 1878–1889.

[6] a) S. De, A. M. Balu, J. C. van der Waal, R. Luque, *ChemCatchem* **2015**, *7*, 1608–1629; b) S. Dutta, A. Bhaumik, K. C. W. Wu, *Energy Environ. Sci.* **2014**, *7*, 3574–3592.

[7] a) N. Brun, S. A. Wohlgemuth, P. Osiceanu, M. M. Titirici, *Green Chem.* **2013**, *15*, 2514; b) S. Gao, H. Fan, S. Zhang, *J. Mater. Chem. A* **2014**, *2*, 18263–18270; c) P. Chen, L.-K. Wang, G. Wang, M.-R. Gao, J. Ge, W.-J. Yuan, Y.-H. Shen, A.-J. Xie, S.-H. Yu, *Energy Environ. Sci.* **2014**, *7*, 4095–4103; d) H. Zhang, Y. Wang, D. Wang, Y. Li, X. Liu, P. Liu, H. Yang, T. An, Z. Tang, H. Zhao, *Small* **2014**, *10*, 3371–3378; e) S. Gao, X. Wei, H. Fan, L. Li, K. Geng, J. Wang, *Nano Energy* **2015**, *13*, 518–526; f) R.

  

Wang, H. Wang, T. Zhou, J. Key, Y. Ma, Z. Zhang, Q. Wang, S. Ji, *J. Power Sources* **2015**, *274*, 741 – 747; g) T. Wu, G. Wang, X. Zhang, C. Chen, Y. Zhang, H. Zhao, *Chem. Commun.* **2015**, *51*, 1334 – 1337; h) S. Gao, K. Geng, H. Liu, X. Wei, M. Zhang, P. Wang, J. Wang, *Energy Environ. Sci.* **2015**, *8*, 221 – 229; i) X. Liu, Y. Zhou, W. Zhou, L. Li, S. Huang, S. Chen, *Nanoscale* **2015**, *7*, 6136 – 6142.

[8] a) W. Luo, B. Wang, C. G. Heron, M. J. Allen, J. Morre, C. S. Maier, W. F. Stickle, X. Ji, *Nano Lett.* **2014**, *14*, 2225 – 2229; b) W. Yang, Y. Zhai, X. Yue, Y. Wang, J. Jia, *Chem. Commun.* **2014**, *50*, 11151 – 11153; c) Q. Liu, Y. Zhou, S. Chen, Z. Wang, H. Hou, F. Zhao, *J. Power Sources* **2015**, *273*, 1189 – 1193; d) Z.-L. Wang, D. Xu, H.-X. Zhong, J. Wang, F.-L. Meng, X.-B. Zhang, *Sci. Adv.* **2015**, *1*, e1400035.

[9] a) M. Harrington, A. Masic, N. Holten-Andersen, J. Waite, P. Fratzl, *Science* **2010**, *328*, 216 – 220; b) H. Ejima, J. Richardson, K. Liang, J. Best, M. van Koeverden, G. Such, J. Cui, F. Caruso, *Science* **2013**, *341*, 154 – 157; c) T. Sileika, D. Barrett, R. Zhang, K. Lau, P. Messersmith, *Angew. Chem. Int. Ed.* **2013**, *52*, 10766 – 10770; *Angew. Chem.* **2013**, *125*, 10966 – 10970; d) J. Guo, Y. Ping, H. Ejima, K. Alt, M. Meissner, J. J. Richardson, Y. Yan, K. Peter, D. von Elverfeldt, C. E. Hagemeyer, F. Caruso, *Angew. Chem. Int. Ed.* **2014**, *53*, 5546 – 5551; *Angew. Chem.* **2014**, *126*, 5652 – 5657.

[10] J. Wei, D. Zhou, Z. Sun, Y. Deng, Y. Xia, D. Zhao, *Adv. Funct. Mater.* **2013**, *23*, 2322 – 2328.

Received: September 26, 2015
Published online: December 11, 2015

  